HHS Public Access

Author manuscript

Small. Author manuscript; available in PMC 2017 January 27.

Published in final edited form as:

Small. 2016 January 27; 12(4): 477–487. doi:10.1002/smll.201501985.

Iron oxide-based nanovector for tumor targeted siRNA delivery in an orthotopic hepatocellular carcinoma xenograft mouse model

Kui Wang,
Department of Materials Science and Engineering, University of Washington, Seattle, WA 98195, USA

Dr. Forrest M. Kievit,
Department of Neurological Surgery, University of Washington, Seattle, WA 98195, USA

Dr. Jonathan G. Sham,
Department of Surgery, University of Washington, Seattle, WA 98195, USA

Mike Jeon,
Department of Materials Science and Engineering, University of Washington, Seattle, WA 98195, USA

Zachary R. Stephen,
Department of Materials Science and Engineering, University of Washington, Seattle, WA 98195, USA

Arvind Bakthavatsalam,
Department of Biochemistry, University of Washington, Seattle, WA, 98195, USA

Dr. James O. Park, and
Department of Surgery, University of Washington, Seattle, WA 98195, USA

Prof. Dr. Miqin Zhang
Department of Materials Science and Engineering, University of Washington, Seattle, WA 98195, USA. Department of Neurological Surgery, University of Washington, Seattle, WA 98195, USA

Abstract

Hepatocellular carcinoma (HCC) is one of the deadliest cancers worldwide. Small interfering RNA (siRNA) holds promise as a new class of therapeutics for HCC as it can achieve sequence-specific gene knockdown with low cytotoxicity. However, the main challenge in the clinical application of siRNA lies in the lack of effective delivery approaches that need to be highly specific and thus incur low or no systemic toxicity. Here, we present a non-viral nanoparticle-based gene carrier that can specifically deliver siRNA to HCC. The nanovector (NP-siRNA-GPC3 Ab) is made of an iron oxide core coated with chitosan-PEG grafted PEI copolymer, which is further functionalized with siRNA and conjugated with a monoclonal antibody (Ab) against human glypican-3 (GPC3) receptor highly expressed in HCC. A rat RH7777 HCC cell line that

Correspondence to: Miqin Zhang.

co-expresses human GPC3 and firefly luciferase (Luc) is established to evaluate the nanovector. The nanoparticle-mediated delivery of siRNA against Luc effectively suppresses Luc expression *in vitro* without notable cytotoxicity. Significantly, NP-siLuc-GPC3 Ab administered intravenously in an orthotopic model of HCC is able to specifically bound to tumor and induce remarkable inhibition of Luc expression. Our findings demonstrate the potential of using this nanovector for targeted delivery of therapeutic siRNA to HCC.

Graphical Abstract

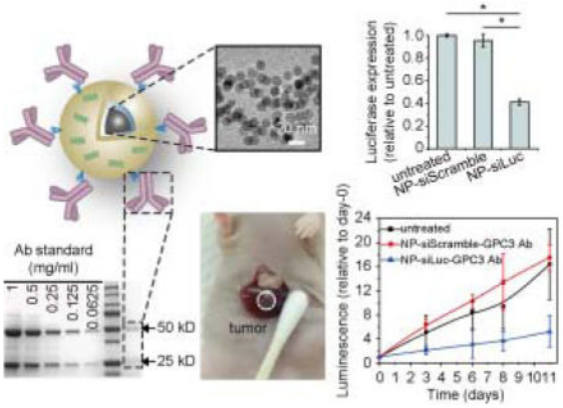

A chitosan-PEG grafted PEI copolymer coated iron oxide nanoparticle leads to efficient siRNA mediated suppression of targeted gene expression with no notable cytotoxicity in hepatocellular carcinoma (HCC) cells *in vitro. In vivo* systemic administration of nanoparticle siRNA complexes incorporated with HCC targeting antibody in mice bearing orthotopic HCC xenografts induces a sustainable gene knock-down.

Keywords

hepatocellular carcinoma; CP-PEI; nanoparticle; RNAi; Glypican-3

1. Introduction

Hepatocellular carcinoma (HCC) is the second-leading cause of cancer-related deaths worldwide, resulting in more than one million deaths annually.[1, 2] Despite its global significance, HCC is understudied compared with other major lethal types of cancer in the US. Although potentially curative treatments such as surgical resection, ablative therapies, and liver transplantation exist,[3] the prognosis remains poor as the majority of patients are diagnosed at an advanced stage and are not candidates for such therapies.[2, 4] Sorafenib, a small molecule tyrosine kinase inhibitor, is currently the only drug approved for the treatment of patients with advanced HCC. However, it prolongs survival by a mere 2–3 months, and has dose-limiting side effects.[5–8] Thereby, there is an urgent need for more effective therapeutic approaches for these patients.

RNA interference (RNAi) mediated by small interfering RNA (siRNA) can silence gene expression in a highly specific manner, and thus holds great promise as a potent inhibitor of

therapeutic targets with low toxicity and a high degree of specificity that is far superior to conventional drugs.[9–11] In fact, many aberrant signal transduction pathways that are associated with tumorigenesis and chemotherapy resistance in HCC have been identified, and RNAi utilized to suppress these targets exhibited encouraging therapeutic effects.[12–14] Although siRNA is powerful gene regulation agents, the efficiency of systemic delivery of siRNA is extremely low due to quick degradation in biological fluids, poor cellular uptake resulted by the inherent physicochemical characteristics of siRNA (i.e., high molecular weight, negative charge, and stiff structure), and inefficient intracellular trafficking to escape from endosomes and release of siRNA in cytoplasm.[15–17]

Nanoparticles as carriers for systemic delivery of synthetic siRNA have gained significant attention.[9, 18] Several nanoscale constructs have been investigated for siRNA delivery to HCC, including cationic polymers, lipid-based, and superparamagnetic nanoparticles.[19–24] Despite many nanoparticle systems have shown promise *in vitro* for targeting tumor cells, their *in vivo* applications and clinical utility have been hindered because of limited potency and poor target specificity, resulting in an unacceptable level of systemic toxicity.[18, 25] As carriers for siRNA delivery, nanoparticles are required to protect siRNA from degradation during transport and overcome extra- and intra- cellular barriers for specific site functions.[18] Compared to other tumors, target-specific delivery of nanoparticles to HCC is especially challenging. Liver cells are filtrated with a large number of Kupffer cells that will quickly take up these nanoparticles before they can reach tumors.[15, 26] In addition, the availability of HCC-specific targeting ligands remains limited although research in finding targeting moieties that recognize HCC-specific cell receptors has been actively pursued in the past decade.[20, 27–30]

In this study, we present a theranostic nanovector (NP-siRNA-GPC3 Ab) and demonstrated that it can specifically and effectively deliver siRNA to HCC through systemic injection in an orthotopic xenograft mouse model. The NP-siRNA-GPC3 Ab is made of an iron oxide core coated with chitosan-PEG grafted polyethyleneimine (PEI) copolymer (CP-PEI) shell and conjugated with a monoclonal antibody (Ab) against human glypican-3 (GPC3) receptor. An iron oxide-based nanoparticle formulation is used here because of its biocompatibility, biodegradability, and inherent superparamagnetic properties that can serve as a magnetic resonance imaging (MRI) contrast agent for disease diagnosis and treatment monitoring, as demonstrated in our previous studies using the same nanoparticle synthesis strategy.[30–33] Chitosan, a natural polymer derived from crustacean shells, has ample functional groups allowing for attachment of functional ligands and cationic polymers for complexing siRNA.[34, 35] The PEG grafted chitosan (herein termed CP) serves as a stabilizer that prevents particle agglomeration. CP-PEI copolymer coated iron oxide nanoparticles has demonstrated their ability to protect siRNA from degradation and facilitate proper intracellular trafficking for safe and effective siRNA delivery.[32] GPC3 Ab is covalently attached to the surface of nanovector to confer the ability of HCC targeting. Recent studies have revealed that GPC3 is a promising receptor for HCC targeting as it is highly expressed in HCC but not in healthy tissues.[36–38] Notably, we have demonstrated the tumor specificity of GPC3 Ab,[30] which has a very high binding affinity (~30 pM) and is internalized by HCC,[39] making it an ideal targeting ligand. A rat RH7777 HCC cell line co-expressing human GPC3 and firefly luciferase (Luc) in orthotopic mouse model is used

to evaluate tumor targeting and NP-siRNA mediated Luc gene silencing due to their ability to form tumors that represent histopathologic features of HCC.

2. Results and discussion

2.1. Nanovector synthesis and characterization

NP-siRNA-GPC3 Ab were synthesized as described in the previous section and illustrated in Figure 1. The presence of CP-PEI copolymer on iron oxide nanoparticles with a siloxane PEG monolayer (IOSPM) was verified by proton NMR (^{1}H-NMR) (Figure 2a). The characteristic ^{1}H-NMR peak at 3.65 ppm (peak I) representing ethylene group (–O–CH_2–CH_2–) of PEG is evidenced on the spectra of IOSPM and IOSPM coated with CP-PEI copolymer (herein termed NP). The ethylenimine (–NH_2–CH_2–CH_2–) repeat unit of PEI at 3.3–3.62 ppm (peak II) and the H3–6 peaks (peak III, δ = 3.68–3.73 ppm; peak IV, δ = 3.9–3.95 ppm) of chitosan on NP spectrum indicate the covalent attachment of CP-PEI on IOSPM. NP was complexed with siRNA at weight ratio (Fe equivalent of NP:siRNA) of 1:2, corresponding to approximately 300 siRNA molecules per NP as determined from calculations of molar masses of NP (~2,000,000 g Fe/mole NP) and siRNA (13,300 g/mole).

Transmission electron microscopy (TEM) images in Figure 2b revealed a spherical morphology of the iron oxide core of NP-siRNA-GPC3 Ab with a size around 10–12 nm, confirming that the iron oxide core sizes remained uniform after copolymer conjugation. Additionally, NP-siRNA-GPC3 Ab was well dispersed in aqueous medium. SDS-PAGE was used to evaluate attachment of GPC3 Ab on NP-siRNA. As shown in Figure 2c, both light and heavy chains of Ab were detected from the purified NP-siRNA-GPC3 Ab under reducing conditions, which confirmed the conjugation of Ab to the NP. Band density quantification revealed there were approximately 26 Ab molecules per NP.

The NP core with copolymer coating of NP-siRNA-GPC3 Ab were characterized by dynamic light scattering (DLS). Both hydrodynamic sizes and zeta potentials of NP, NP-siRNA, and NP-siRNA-GPC3 Ab were determined (Figure 2d). No apparent change in size was observed after siRNA binding (39.87 ± 0.83 nm *vs.* 39.65 ± 0.70 nm), suggesting the strong complexing capacity of NP. NP slightly increased in size to 41.02 ± 0.41 nm after GPC3 Ab conjugation. The size of NP has a dramatic effect on nonspecific uptake by off-target cells in the body. In order to successfully reach the tumor site, NP has to overcome multiple physiological barriers including the liver, kidneys, and spleen. The hydrodynamic size of NP should be between 10–100 nm to avoid elimination by these organs.[25] Moreover, our NP-siRNA-GPC3 Ab is smaller than 60 nm, which is expected to have better penetration from blood vessels into tumor.[40]

Zeta potential is another important physicochemical property for DNA/siRNA delivery applications.[41] The positive surface charge correlates with the capacities of NP to electrostatically complex and deliver siRNA into cells. Our base NP exhibited a zeta potential value of 27.85 ± 2.33 mV (Figure 2d). After siRNA complexation (NP-SiRNA), the zeta potential showed little change (27.30 ± 0.28 mV), consistent with the hydrodynamic size measurement which showed little change before and after siRNA complexation. After Ab attachment, the zeta potential of NP-siRNA-GPC3 Ab decreased to 22.85 ± 2.62 mV.

This was likely caused by the addition of the PEG linker and Ab, which could both shield the charge of the NP.

The gel retardation assay was utilized to further demonstrate full siRNA binding in NP. As shown in the gel image (left panel of Figure S1), the siRNA band was not visible when complexed with NP, suggesting the fully encapsulation of siRNA in the copolymer coating of the NP. siRNA was released from NP when treated with heparin, an electrostatic disrupting agent, as visualized by the siRNA band on the gel (right panel of Figure S1). Overall, the characterization of NP-siRNA-GPC3 Ab suggested that this NP system should function well as a vehicle for delivery of siRNA into HCC.

2.2. Development of GPC3 and Luc co-expressing RH7777 (RH7777-Luc-GPC3) cells

To enable targeted siRNA delivery using our previously developed anti-GPC3 Ab,[30] human GPC3 was stably transfected into RH7777 cells. Additionally, we stably transfected RH7777 cells with Luc for proof-of-concept knockdown experiments using our nanovector. RH7777 cells were chosen because of their ability to form tumors in the livers of athymic nude mice that represent histopathologic features of HCC.

Here we used siLuc as our therapeutic siRNA and scramble siRNA (siScramble) as control siRNA. Prior to evaluating *in vitro* and *in vivo* knockdown efficiency of NP-siLuc, expression level of Luc and GPC3 in the established RH7777-Luc-GPC3 cells were measured. The *in vitro* Luc assay revealed a 1224-fold higher luminescent signal in RH7777-Luc-GPC3 cells as compared to native RH7777 cells (Figure 3a). Surface expressed GPC3 antigen on RH7777-Luc-GPC3 cells were analyzed by flow cytometry. As shown in Figure 3b, flow cytometric analysis revealed a distinct GPC3 positive cell population with significantly higher fluorescence intensity when compared to the unstained and non-targeting Ab controls. Taken together, these results verified the successful generation of a Luc and GPC3 co-expressing RH7777 cell line.

2.3. *In vitro* knockdown of Luc

After successfully establishing RH7777 cells that co-express Luc and GPC3, we evaluated gene-silencing efficacy of NP-siLuc *in vitro*. Forty-eight hours after NP-siLuc transfection, transient Luc expression in RH7777-Luc-GPC3 cells was measured at both mRNA and protein levels by quantitative RT-PCR (qRT-PCR) and Luc assays, respectively. As shown in Figure 4a and 4b, NP-siLuc exposure resulted in a 66% reduction in mRNA abundance, corresponding to a 79% suppression of Luc activity in RH7777-Luc-GPC3 cells. In contrast, no inhibition of Luc expression was observed from untreated or NP-siScramble treated cells.

Upon uptake by cells, NP-siRNA need to access cytoplasm to initiate RNAi. To further illustrate the mechanism of the nanovector-mediated gene knock-down, we investigated the escape of NP-siRNA from endosomes using an endosomal integrity assay.[42] Calcein fluorescence (green) was barely detectable in RH7777-Luc-GPC3 cells indicating the integrity of endosomes while calcein fluorescence was observed throughout the cells contain both NP-siRNA and calcein (Figure 4c). Distribution of NP-siRNA in RH7777-Luc-GPC3 cells was detected using fluorophore-labeled siScramble. As shown in Figure 4d, fluorescence signal from NP-siRNA (red) could be observed throughout the cytoplasm,

supporting the calcein endosomal integrity assay results that NP-siRNA was able to escape from endosomes and readily access the cytoplasm of cells. Once NP-siRNA was internalized into the cells through endocytosis, the PEI on NP copolymer coating can trigger endosomal escape through the proton sponge effect, where the influx of protons and counter-ions promotes the swelling and rupture of endosomes and the release of NP-siRNA complex into the cytoplasm.[43]

We also measured NP-siRNA-associated toxicity using the alamar blue (AB) assay. Compared to the untreated control, approximately 80% cell viability was observed at 48 hr after transfection (Figure 4e) indicating the biocompatibility of the NP. These results demonstrate that NP-siRNA can efficiently suppress a target gene with limited cellular toxicity in cultured HCC cells.

2.4. Establishment and characterization of orthotopic RH7777-Luc-GPC3 xenograft

Having demonstrated that *in vitro* delivery of siLuc using our NP could produce effective gene silencing, we evaluated the efficacy of NP-siLuc mediated Luc suppression *in vivo*. We developed RH7777-Luc-GPC3 orthotopic xenografts as illustrated in Figure 5a. Successful hepatic grafting with a 5 mm tumor nodule with well-defined margins was observed during surgery. The histological characteristics of tumor tissues were analyzed by H&E staining. As shown in Figure 5b, a moderately well-defined tumor that is separated from normal liver is observed in the enlarged image. The marked nuclear crowding and typical trabecular growth pattern are representative histopathologic features of HCC.[44] This demonstrates the successful grafting of RH7777-Luc-GPC3 orthotopic xenograft tumors.

To verify GPC3 expression in the tumors, we isolated tumor cells and analyzed their surface GPC3 expressing using flow cytometry. As shown in Figure 5c, RH7777 cells with or without anti-GPC3 Ab staining show similar fluorescence intensity, suggesting the absence of GPC3 antigen expression. As a comparison, a distinct population of GPC3-positive cells was observed in isolated RH7777-Luc-GPC3 tumor cells, demonstrating that the RH7777-Luc-GPC3 xenograft tumors retained surface GPC3 antigen expression *in vivo*, and confirming that this model can be used for the study of GPC3 Ab-guided siRNA delivery *in vivo*.

2.5. *In vivo* tumor targeted delivery of siRNA

Administration of siRNA specifically into tumor site and the correct intracellular location is essential for gene silencing activity. NP-mediated DNA/siRNA delivery can be enhanced specifically in the tumor through attachment of targeting ligands on the surface of the NP.[31, 32] To enable tumor targeted delivery of siRNA *in vivo*, we incorporated GPC3 Ab into NP-siRNA (hereafter NP-siRNA-GPC3 Ab). The localization of NP-siRNA-GPC3 Ab to the orthotopic HCC was evaluated using Dy677-labeled siScramble complexed into NP. Mice were administered with NP-siRNA-GPC3 Ab via tail vein injection and imaged using a Xenogen IVIS Imaging system at 4, 24, 48, 72, and 120 hr post-injection with untreated mice as control (Figure 6a). Bioluminescent imaging revealed the tumor location while fluorescence imaging showed the distribution of Dy677-labeled siRNA.

As shown in Figure 6a, Dy677 fluorescence (red) from Dy677-labeled siRNA loaded NP was detectable in liver at 4 hr after injection. The overlap of the fluorescence and luminescence (blue) from tumors indicates accumulation of NP in the xenograft tumors. A decay of fluorescence signal as a function of time was also observed, most likely a reflection of the elimination of NP through clearance organs. NP-siRNA-GPC3 Ab remained detectable at 120 hr after injection, indicating the prolonged retention of NP-siRNA-GPC3 Ab in tumors. To further confirm the presence of NP-siRNA-GPC3 Ab within the tumors, the tumors were harvested and tumor sections were imaged by confocal fluorescent microscopy. There was no Dy677 fluorescence observed in untreated control animals whereas NP-siRNA-GPC3 Ab produced appreciable fluorescence in tumor regions (Figure 6b). In addition, Dy677 fluorescence was seen near the nucleus suggesting NP-siRNA-GPC3 Ab was able to deliver siRNA to the perinuclear region site of action. No accumulation of NP-siRNA-GPC3 Ab was detected in non-neoplastic tissue, including liver, spleen, kidney, and lung 5 days after NP injection (Figure S2), which further confirms the targeting capability of NP-siRNA-GPC3 Ab to HCC. These findings demonstrate that our NP platform can achieve targeted siRNA delivery to tumor tissue through intravenous administration.

2.6. NP-mediated Luc silencing *in vivo*

To determine whether the siRNA delivered to the tumor site was bioactive and could knock down gene expression, siLuc formulated in the nanovector was administered at 20 μg siRNA per animal intravenously daily for five days. Luc expression was assessed using a Xenogen IVIS Imaging system on 3, 6, 8, and 11 days after the first NP-siRNA-GPC3 Ab injection, as shown in the scheme in Figure 7a. A significantly decreased bioluminescence signal (from tumor cells) in NP-siLuc-GPC3 Ab treated mice was observed as compared to untreated mice and NP-siScramble-GPC3 Ab treated mice (Figure 7b). The normalization of the bioluminescent signal revealed that the untreated and control siRNA (siScramble) treated animals indicated a continuously elevated luminescence signal, representing the tumor cell proliferation. As a comparison, NP-siLuc-GPC3 Ab induced a dramatically retarded increase of luminescence signal, with approximately 4-times lower than untreated and control siRNA treated animals on day 11 (Figure 7c). In addition, both untreated and control siRNA treated animals showed similar tumor bioluminescence levels, indicating the effect was specific to siRNA delivery and not a non-specific reduction in tumor growth or Luc expression levels caused by the NP or GPC3 Ab themselves.

The tumor accumulation observed with fluorophore labeled NP-siRNA-GPC3 Ab may occur through both GPC3 Ab mediated targeting and passive tumor accumulation through the “enhanced permeability and retention” (EPR) effect.[45, 46] NP likely enter the tumor site though the EPR effect followed by active distribution throughout the tumor from the tumor targeting ligand.[47, 48] Without targeting ligand, positively charged NPs have strong affinity to both extracellular matrix (ECM) and target cells.[49] In contrast, accumulation of NP-siRNA-GPC3 Ab in tumor can be enhanced by GPC3 Ab. In the current study, the *in vivo* gene-silencing activity parallels tumor accumulation and intracellular uptake of NP complex. A sustainable reduction in Luc activity was induced by NP-siLuc treatment. This provides strong evidence that our nanovector is a suitable nanocarrier for siRNA delivery to HCC.

The use of siRNA against therapeutic targets will be the next step in the development of these nanovector for improved HCC therapy. We have found therapeutic targets that are effective alone[50] as well as those that can enhance the effects of conventional treatments.[42] Additionally, the targeting capacity of our nanovector may allow them to potentially reach any organ system with HCC involvement, which allows treatment of disseminated HCC.[51, 52] This could provide a more effective option for patients with untreatable HCC.

3. Conclusion

We have reported the rational design and synthesis of an iron oxide-based nanoparticle coated with CP-PEI copolymer and conjugated with an anti-GPC3 Ab tumor targeting ligand for specific and effective siRNA delivery to HCC. The nanovector exhibited appropriate physiochemical properties required for systemic siRNA delivery to tumor. We showed that the nanovector loaded with siRNA could successfully lower expression levels of target genes (Luc reporter) *in vitro* without evident associated toxicity. We further demonstrated that the intravenous administration of HCC targeted NP-siRNA-GPC3 Ab resulted in nanovector accumulation in RH7777-Luc-GPC3 orthotopic HCC and induced significantly decreased Luc activity. Overall, our results demonstrated the ability of this NP platform to overcome intra- and extra- cellular barriers and its promise in delivering siRNA for HCC treatment.

4. Experimental Section

Materials

All chemicals were purchased from Sigma-Aldrich unless otherwise specified, and tissue culture reagents were purchased from Life Technologies unless otherwise specified.

Nanovector synthesis

The preparation of NP-siRNA-GPC3 Ab is outlined in Figure 1. CP, CP-PEI copolymer, and iron oxide nanoparticles with a siloxane PEG monolayer (IOSPM) were synthesized as described previously.[53–55] The IOSPM was coated with CP-PEI copolymer through crosslinking SIA and Traut's regents (Molecular Biosciences) before purification using a S-200 sephacryl resin (GE Healthcare) equilibrated with 20 mM HEPES buffer (pH 7.4) (Figure 1a). IOSPM coated with CP-PEI copolymer, herein termed NP, were complexed with siRNA at weight ratio (Fe equivalent of NP:siRNA) of 1:2 in 20 mM HEPES buffer (pH 7.4), and incubated for 20 min at room temperature to allow formation of NP-siRNA complexes. Subsequently, GPC3 Ab was conjugated to NP-siRNA using a heterobifunctional PEG linker, NH_S-PEG_{12}-maleimide. Briefly, GPC3 Ab was reacted with excess Traut's reagent in thiolation buffer (pH 8.0) for 1 hr in the dark at room temperature to form Ab Traut's. Unreacted Traut's reagent was removed through Zeba spin columns (Life Technologies). NP-siRNA was reacted with NHS-PEG_{12}-maleimide (Life Technologies) in the dark at room temperature with gentle rocking for 30 min before removing unreacted linker through Zeba spin columns. The thiolated Ab was mixed with thiol-reactive NP-siRNA (2 mg Ab per 1 mg NP-siRNA) and allowed to react for 1 hr in the dark at room temperature with gentle rocking. Unreacted Ab was removed from NP

conjugated Ab through size exclusion chromatography in S-200 sephacryl resin to obtain pure NP-siRNA-GPC3 Ab (Figure 1b).

Nanovector characterization

For proton NMR (^{1}H-NMR) analysis, 50 μg (Fe) of IOSPM and NP were lyophilized to remove water. 30 μl of DCl and 870 μl of D_2O were added to the lyophilized NP to dissolve the iron core leaving free polymer coating in solution. 1.72 mg of trimethylsilyl propionate in 100 μl D_2O was added as internal reference. ^{1}H-NMR spectra were obtained using a Bruker Avance 300 spectrometer operating at 300 MHz (1H) and 325 K (number of scans = 128, acquisition time = 3s, delay (D1) = 1s).

For transmission electron microscopy (TEM) analysis, NP-siRNA-GPC3 Ab was diluted to 100 μg/mL in deionized water and 5 μL of the dilute solution were placed on a formvar/carbon coated 300 mesh copper grid (Ted Pella). After 5 min, the NP solution was removed and the grid was allowed to dry overnight before imaging using a Tecnai G2 F20 electron microscope (FEI) operating at a voltage of 200 kV. Hydrodynamic size and zeta potential analyses were acquired in HEPES buffer (pH 7.4) using a DTS Zetasizer Nano (Malvern Instruments).

GPC3 Ab after conjugated onto the NP-siRNA surface was detected by a sodium dodecyl sulfate polyacrylamide gel electrophoresis (SDS-PAGE) in comparison with free GPC3 Ab. A Precision Plus Protein™ Dual Color Standard (Bio-Rad) was used as molecular weight marker. The gel was run under reducing conditions by using a Mini PROTEAN 3 Cell electrophoresis unit (Bio-Rad) at a constant voltage mode of 100 V in a Tris/glycine/SDS buffer. The gel was then stained with Coomassie Brilliant Blue solution (Bio-Rad) and imaged with a Bio-Rad Universal Hood II Gel Doc System. NP-siRNA-GPC3 Ab was also evaluated for their possession of Ab by measurement of their absorption at $OD_{280\ nm}$ using a SpectraMax i3 multi-mode microplate reader (Molecular Devices).

siRNA binding was characterized using gel retardation assay. NP-siRNA complexes containing 1 μg siRNA were prepared at NP:siRNA weight ratios of 1:2 in 20 mM HEPES buffer (pH 7.4). The complex were treated with heparin (1000 units/ml, 50 μL Heparin/1 μg siRNA) and incubated for 30 min at room temperature to block the electrostatic interaction between NP and siRNA. Both heparin-treated and untreated complexes were loaded onto a native polyacrylamide gel for electrophoresis for about 30 min. After staining the gel with 0.5 μg/ml ethidium bromide, free-siRNA was detected using a Gel Doc XR (Bio-Rad).

Cell culture

Rat RH7777 HCC cells were purchased from American Type Culture Collection (ATCC no. CRL-1601) and cultured at 37°C in a humidified atmosphere with 5% CO_2 using Dulbecco's modified Eagle's Medium (DMEM) supplemented with 10% fetal bovine serum and 1% antibiotic-antimycotic.

GPC3 and Luc co-expressing RH7777 (RH7777-Luc-GPC3) cells were generated by transfecting previously established Luc-expressing RH7777 cells[38] with pLX304-BLAS-V5-GPC3 (Life Technologies) using Lipofectamine 2000 (Life Technologies) following the

manufacture's protocol. Three days after transfection, regular DMEM was replaced by DMEM containing 2.5 μg/ml blasticidin. Cells were maintained in the selective medium for additional three weeks prior to sorting with a BD FACSAria™ II cell sorter (BD Biosciences). The stably transfected RH7777-Luc-GPC3 cells were cultured in complete medium supplemented with 2.5 μg/ml blasticidin.

Surface GPC3 antigen expression on the established RH7777-Luc-GPC3 cells was analyzed by flow cytometry. RH7777-Luc-GPC3 cells were incubated with mouse anti-GPC3 Ab (1 mg/ml, 1:50 dilution) at 4°C for 30 min, and then probed with FITC conjugated rabbit anti-mouse secondary Ab (Abcam, 1:100 dilution) at 4°C for 30 min. Cells were then washed, collected and analyzed with a FACSCanton™ II flow cytometer (BD Biosciences). Data were analyzed with FlowJo (Ashland).

In vitro cell transfection

Twenty-four hours after plating RH7777-Luc-GPC3 cells at a concentration of 25,000 cells/ml, transfection was performed by replacing cell culture medium with 1 ml of NP-siRNA complex-containing medium (50 nmol siRNA per well). After 4 hr of transfection, NP-siRNA complex-containing medium was removed and replaced with fresh DMEM. Firefly luciferase gene-targeting siRNA (siLuc) and scramble siRNA (siScramble) were purchased from Dharmacon Research Inc.

Endosomal escape was evaluated using an endosomal integrity assay.[42] In brief, RH7777-Luc-GPC3 cells were co-incubated with NP-siRNA and membrane impermeable dye calcein (0.25 mM). Excess dye was washed off after 2 hr incubation. Cells were fixed and nuclei were stained with DAPI prior to imaging by fluorescence microscopy.

To evaluate NP-siRNA uptake, RH7777-Luc-GPC3 cells were transfected with NP complexed with Dy677-labeled siScramble (Dharmacon Research Inc). Twelve hours later, cells were fixed in 4% formaldehyde and nuclei were stained with DAPI prior to imaging using fluorescence microscopy.

Cell viability assay

The effect of NP-siRNA on RH7777-Luc-GPC3 cell viability was determined using the alamar blue (AB) assay following the manufacture's protocol (Life Technologies). Briefly, cells were plated and transfected as described. After treatment, cells were washed with PBS three times before adding 10% AB solution in DMEM medium to the wells. Cells were incubated for 1 hr, then the AB solution was transferred to a 96-well plate, and the fluorescent emissions at an excitation wavelength of 550 nm and an emission wavelength of 590 nm were read with a microplate reader.

Quantitative RT-PCR (qRT-PCR)

RNA was extracted from cells 48 hr after siRNA transfection using the Qiagen RNeasy kit. cDNA was prepared using the iScript cDNA Synthesis kit (Bio-Rad) following the manufacturer's protocol, which was then used as a template for PCR. qRT-PCR was used to evaluate the relative expression levels of Luc utilizing rat glyceraldehyde 3-phosphate

dehydrogenase (GAPDH) as a control. SYBR Green PCR Master mix (Bio-Rad) was used for template amplification with a primer for each of the transcripts in a Bio-Rad CFX96 real-time PCR detection system. Quantitative amplification was monitored by the level of fluorescence reflecting the cycle number at the detection threshold (crossing point) using a standard curve. Thermocycling for all targets was carried out in a solution of 20 μl containing 0.5 μM primers (Integrated DNA Technologies) and 4 pg of cDNA from the reverse transcription reaction under following conditions: 95°C for 2 min, 40 cycles of denaturation (15 sec, 95°C), annealing (30 sec, 58°C), and extension (30 sec, 72°C). The primers used for GAPDH and Luc were forward: 5′-GACATGCCGCCTGGAGAAAC-3′/ reverse: 5′-AGCCCAGGATGCCCTTTAGT-3′ and forward: 5′-ATTACACCCGAGGGGGATGA-3′/reverse: 5′-TCTCACACACAGTTCGCCTC-3′, respectively.

Luc activity quantification

In vitro measurement of Luc activity was conducted using Luc assay following the manufacture's protocol (Promega). Briefly, 50,000 cells were collected and washed with PBS three times before lysed by 0.1% Triton-X. 200 μl of cell lysis were reacted with 50 μl luciferin, and read with a microplate reader. Protein was quantified by Bradford assay (Bio-Rad) following the manufacture's protocol.

Animal model

All animal studies were performed in accordance with the University of Washington Office of Animal Welfare guidelines for the humane use of animals, and all procedures were reviewed and approved by the Institutional Animal Care and Use Committee. For the orthotopic xenograft model, 8-week-old female athymic Nu/J mice (Jackson Laboratories) were anesthetized using 1.5% inhaled isoflurane and the left lobe of the liver was exposed through an upper midline laparotomy. RH7777-Luc-GPC3 cells (1×10^6) in 50 μL of DMEM containing 50% Matrigel (BD Biosciences) were injected into the subcapsular space of the left lobe. Two weeks after injection, a 75 mg/kg intraperitoneal injection of VivoGlo luciferin (Promega) was administered and imaging was performed using an IVIS Lumina II system (PerkinElmer) to monitor the growth of intrahepatic tumors.

To analyze the GPC3 antigen expression on RH7777-Luc-GPC3 xenograft, tumors were harvested two weeks after implantation. Tumor cells were dissociated and passed through a 70 μm cell strainer (Thermo Fisher Scientific) to acquire single cell suspension. They were then subjected to anti-GPC3 Ab staining as described previously, and analyzed by flow cytometry using a FACSCanton™ II flow cytometer (BD Biosciences). Data were analyzed with FlowJo (Ashland).

Histological analysis

After NP treatment, RH7777-Luc-GPC3 liver tumor tissues were fixed in 4% formaldehyde for 24 hr and placed in 30% sucrose until fully saturated. The tissues were subsequently cut into small pieces and frozen in OCT embedding medium (Sakura) at −80°C. Frozen sections (8 μm thickness) were stained with DAPI (Life Technologies) and photographed under a Zeiss 510 META confocal fluorescence microscope.

Statistical Analysis

All the data were statistically analyzed to express the mean value ± standard deviation (SD) of the mean. An unpaired, 2-tailed Student's *t* test was used, with a *P* value of less than 0.05 considered statistically significant.

Supplementary Material

Refer to Web version on PubMed Central for supplementary material.

Acknowledgments

We acknowledge financial support from NIH grants R01CA161953 and R01CA134213 to M. Z.. K. W. acknowledges support from the College of Engineering Dean's Fellowship (the Scott Fellowship and the Marsh Fellowship) at University of Washington. F. M. K. acknowledges support from an NIH training grant (T32CA138312) and an American Brain Tumor Association fellowship in honor of Susan Kramer. We thank the Department of Pathology at the University of Washington for H&E staining services. We acknowledge the use of the confocal microscope at the Keck Microscopy Facility at the University of Washington. We also thank Andrew (Hyung Jun) Chang, Yayi Deng, and Joshua J. Lim for laboratory assistance.

References

1. Roberts LR. N Engl J Med. 2008; 359:420. [PubMed: 18650519]
2. Forner A, Llovet JM, Bruix J. Lancet. 2012; 379:1245. [PubMed: 22353262]
3. El-Serag HB. N Engl J Med. 2011; 365:1118. [PubMed: 21992124]
4. Villanueva A, Hernandez-Gea V, Llovet JM. Nat Rev Gastroenterol Hepatol. 2013; 10:34. [PubMed: 23147664]
5. Llovet JM, Ricci S, Mazzaferro V, Hilgard P, Gane E, Blanc JF, de Oliveira AC, Santoro A, Raoul JL, Forner A, Schwartz M, Porta C, Zeuzem S, Bolondi L, Greten TF, Galle PR, Seitz JF, Borbath I, Haussinger D, Giannaris T, Shan M, Moscovici M, Voliotis D, Bruix J, Grp SIS. N Engl J Med. 2008; 359:378. [PubMed: 18650514]
6. Xie B, Wang D, Spechler S. Dig Dis Sci. 2012; 57:1122. [PubMed: 22451120]
7. Benson AB, Abrams TA, Ben-Josef E, Bloomston PM, Botha JF, Clary BM, Covey A, Curley SA, D'Angelica MI, Davila R, Ensminger WD, Gibbs JF, Laheru D, Malafa MP, Marrero J, Meranze SG, Mulvihill SJ, Park JO, Posey JA, Sachdev J, Salem R, Sigurdson ER, Sofocleous C, Vauthey JN, Venook AP, Goff LW, Yen Y, Zhu AX. J Natl Compr Cancer Network. 2009; 7:350.
8. Bruix J, Raoul JL, Sherman M, Mazzaferro V, Bolondi L, Craxi A, Galle PR, Santoro A, Beaugrand M, Sangiovanni A, Porta C, Gerken G, Marrero JA, Nadel A, Shan M, Moscovici M, Voliotis D, Llovet JM. J Hepatol. 2012; 57:821. [PubMed: 22727733]
9. Davis ME, Zuckerman JE, Choi CHJ, Seligson D, Tolcher A, Alabi CA, Yen Y, Heidel JD, Ribas A. Nature. 2010; 464:1067. [PubMed: 20305636]
10. Kouraklis G. Dig Dis Sci. 2000; 45:1045. [PubMed: 10877214]
11. Flintoft L. Nat Rev Genet. 2007; 8:908.
12. Zender L, Xue W, Zuber J, Semighini CP, Krasnitz A, Ma B, Zender P, Kubicka S, Luk JM, Schirmacher P, McCombie WR, Wigler M, Hicks J, Hannon GJ, Powers S, Lowe SW. Cell. 2008; 135:852. [PubMed: 19012953]
13. Tabernero J, Shapiro GI, LoRusso PM, Cervantes A, Schwartz GK, Weiss GJ, Paz-Ares L, Cho DC, Infante JR, Alsina M, Gounder MM, Falzone R, Harrop J, White ACS, Toudjarska I, Bumcrot D, Meyers RE, Hinkle G, Svrzikapa N, Hutabarat RM, Clausen VA, Cehelsky J, Nochur SV, Gamba-Vitalo C, Vaishnaw AK, Sah DWY, Gollob JA, Burris HA. Cancer Discovery. 2013; 3:406. [PubMed: 23358650]
14. Rudalska R, Dauch D, Longerich T, McJunkin K, Wuestefeld T, Kang TW, Hohmeyer A, Pesic M, Leibold J, von Thun A, Schirmacher P, Zuber J, Weiss KH, Powers S, Malek NP, Eilers M, Sipos B, Lowe SW, Geffers R, Laufer S, Zender L. Nat Med. 2014; 20:1138. [PubMed: 25216638]

15. Xu CR, Lee SA, Chen X. Recent Patents Anti-Canc Drug Discov. 2011; 6:106.
16. Li JM, Zhao MX, Su H, Wang YY, Tan CP, Ji LN, Mao ZW. Biomaterials. 2011; 32:7978. [PubMed: 21784514]
17. Whitehead KA, Langer R, Anderson DG. Nat Rev Drug Discovery. 2009; 8:129. [PubMed: 19180106]
18. Pecot CV, Calin GA, Coleman RL, Lopez-Berestein G, Sood AK. Nat Rev Cancer. 2011; 11:59. [PubMed: 21160526]
19. Hsu, S-h; Yu, B.; Wang, X.; Lu, Y.; Schmidt, CR.; Lee, RJ.; Lee, LJ.; Jacob, ST.; Ghoshal, K. Nanomedicine. 2013; 9:1169. [PubMed: 23727126]
20. Wu C, Gong F, Pang P, Shen M, Zhu K, Cheng D, Liu Z, Shan H. PLoS ONE. 2013; 8:e66416. [PubMed: 23922634]
21. Chen J, Zhu S, Tong L, Li J, Chen F, Han Y, Zhao M, Xiong W. BMC Cancer. 2014; 14:114. [PubMed: 24555445]
22. Dudek H, Wong DH, Arvan R, Shah A, Wortham K, Ying B, Diwanji R, Zhou W, Holmes B, Yang H, Cyr WA, Zhou Y, Shah A, Farkiwala R, Lee M, Li Y, Rettig GR, Collingwood MA, Basu SK, Behlke MA, Brown BD. Mol Ther. 2014; 22:92. [PubMed: 24089139]
23. Bogorad RL, Yin H, Zeigerer A, Nonaka H, Ruda VM, Zerial M, Anderson DG, Koteliansky V. Nat Commun. 2014; 5
24. Ding Y, Wang W, Feng M, Wang Y, Zhou J, Ding X, Zhou X, Liu C, Wang R, Zhang Q. Biomaterials. 2012; 33:8893. [PubMed: 22979990]
25. Kievit FM, Zhang M. Acc Chem Res. 2011; 44:853. [PubMed: 21528865]
26. Ruoslahti E, Bhatia SN, Sailor MJ. J Cell Biol. 2010; 188:759. [PubMed: 20231381]
27. Liu YJ, Chen ZJ, Liu CX, Yu DX, Lu ZJ, Zhang N. Biomaterials. 2011; 32:5167. [PubMed: 21521627]
28. Diez S, Navarro G, de Ilarduya CT. J Gene Med. 2009; 11:38. [PubMed: 19021130]
29. Liu P, Li Z, Zhu M, Sun Y, Li Y, Wang H, Duan Y. J Mater Sci: Mater Med. 2010; 21:551. [PubMed: 19921404]
30. Park JO, Stephen Z, Sun C, Veiseh O, Kievit FM, Fang C, Leung M, Mok H, Zhang M. Mol Imaging. 2011; 10:69. [PubMed: 21303616]
31. Kievit FM, Veiseh O, Fang C, Bhattarai N, Lee D, Ellenbogen RG, Zhang M. ACS Nano. 2010; 4:4587. [PubMed: 20731441]
32. Veiseh O, Kievit FM, Fang C, Mu N, Jana S, Leung MC, Mok H, Ellenbogen RG, Park JO, Zhang M. Biomaterials. 2010; 31:8032. [PubMed: 20673683]
33. Sun CR, Du K, Fang C, Bhattarai N, Veiseh O, Kievit F, Stephen Z, Lee DH, Ellenbogen RG, Ratner B, Zhang MQ. ACS Nano. 2010; 4:2402. [PubMed: 20232826]
34. Howard KA, Rahbek UL, Liu X, Damgaard CK, Glud SZ, Andersen MO, Hovgaard MB, Schmitz A, Nyengaard JR, Besenbacher F, Kjems J. Mol Ther. 2006; 14:476. [PubMed: 16829204]
35. Rinaudo M. Prog Polym Sci. 2006; 31:603.
36. Nakatsura T, Yoshitake Y, Senju S, Monji M, Komori H, Motomura Y, Hosaka S, Beppu T, Ishiko T, Kamohara H, Ashihara H, Katagiri T, Furukawa Y, Fujiyama S, Ogawa M, Nakamura Y, Nishimura Y. Biochem Biophys Res Commun. 2003; 306:16. [PubMed: 12788060]
37. Capurro MI, Xiang YY, Lobe C, Filmus J. Cancer Res. 2005; 65:6245. [PubMed: 16024626]
38. Sham JG, Kievit FM, Grierson JR, Miyaoka RS, Yeh MM, Zhang M, Yeung RS, Minoshima S, Park JO. J Nucl Med. 2014; 55:799. [PubMed: 24627434]
39. Sham JG, Kievit FM, Grierson JR, Chiarelli PA, Miyaoka RS, Zhang M, Yeung RS, Minoshima S, Park JO. J Nucl Med. 2014; 55:2032. [PubMed: 25359880]
40. Popović Z, Liu W, Chauhan VP, Lee J, Wong C, Greytak AB, Insin N, Nocera DG, Fukumura D, Jain RK, Bawendi MG. Angew Chem, Int Ed. 2010; 49:8649.
41. Doane TL, Chuang CH, Hill RJ, Burda C. Acc Chem Res. 2012; 45:317. [PubMed: 22074988]
42. Kievit FM, Stephen ZR, Wang K, Dayringer CJ, Sham JG, Ellenbogen RG, Silber John R, Zhang M. Mol Oncol. 2015; 9:1071. [PubMed: 25681012]
43. Godbey WT, Wu KK, Mikos AG. J Controlled Release. 1999; 60:149.

44. Kojiro M. Best Pract Res, Clin Gastroenterol. 2005; 19:39. [PubMed: 15757804]
45. Maeda H, Bharate GY, Daruwalla J. Eur J Pharm Biopharm. 2009; 71:409. [PubMed: 19070661]
46. Cho KJ, Wang X, Nie SM, Chen Z, Shin DM. Clin Cancer Res. 2008; 14:1310. [PubMed: 18316549]
47. Jokerst JV, Lobovkina T, Zare RN, Gambhir SS. Nanomedicine. 2011; 6:715. [PubMed: 21718180]
48. Albanese A, Tang PS, Chan WCW. Annu Rev Biomed Eng. 2012; 14:1. [PubMed: 22524388]
49. Wang K, Kievit FM, Florczyk SJ, Stephen ZR, Zhang M. Biomacromolecules. 2015
50. Wang K, Park JO, Zhang M. J Gene Med. 2013; 15:42. [PubMed: 23319157]
51. Budhu A, Jia HL, Forgues M, Liu CG, Goldstein D, Lam A, Zanetti KA, Ye QH, Qin LX, Croce CM, Tang ZY, Wang XW. Hepatology. 2008; 47:897. [PubMed: 18176954]
52. Ye QH, Qin LX, Forgues M, He P, Kim JW, Peng AC, Simon R, Li Y, Robles AI, Chen Y, Ma ZC, Wu ZQ, Ye SL, Liu YK, Tang ZY, Wang XW. Nat Med. 2003; 9:416. [PubMed: 12640447]
53. Fang C, Bhattarai N, Sun C, Zhang M. Small. 2009; 5:1637. [PubMed: 19334014]
54. Kievit FM, Veiseh O, Bhattarai N, Fang C, Gunn JW, Lee D, Ellenbogen RG, Olson JM, Zhang M. Adv Funct Mater. 2009; 19:2244. [PubMed: 20160995]
55. Bhattarai N, Ramay HR, Gunn J, Matsen FA, Zhang M. J Controlled Release. 2005; 103:609.

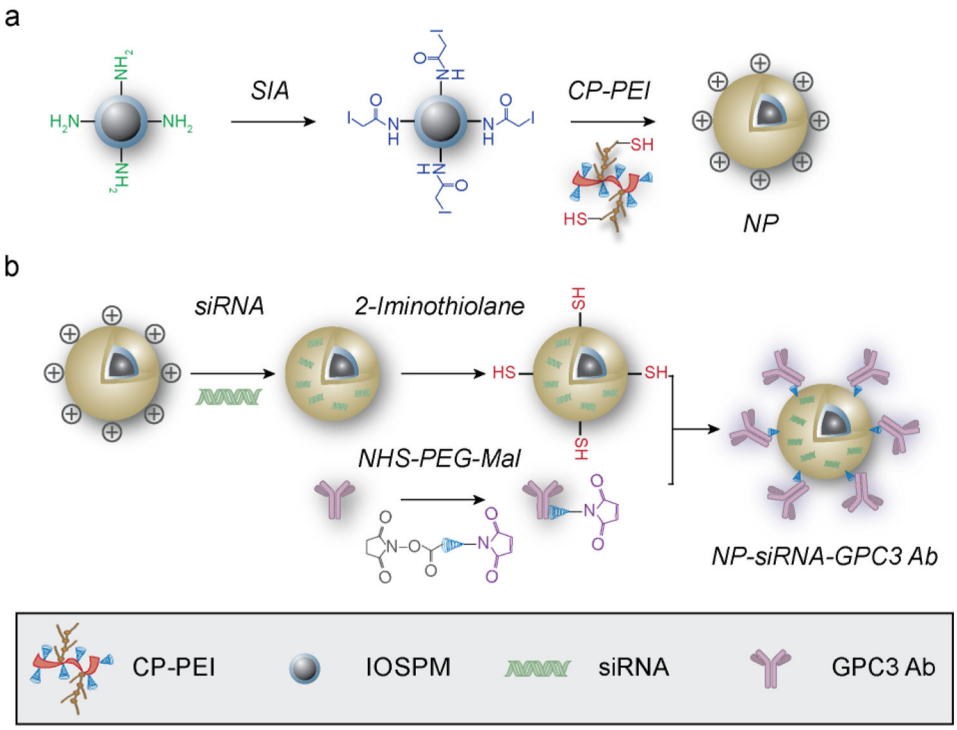

Figure 1.

Schematic of NP-siRNA-GPC3 Ab synthesis. (a) Modification of IOSPM with CP-PEI to produce our NP. (b) NP-siRNA complexation and subsequent conjugation with GPC3 Ab to form fully functionalized NP-siRNA-GPC3 Ab.

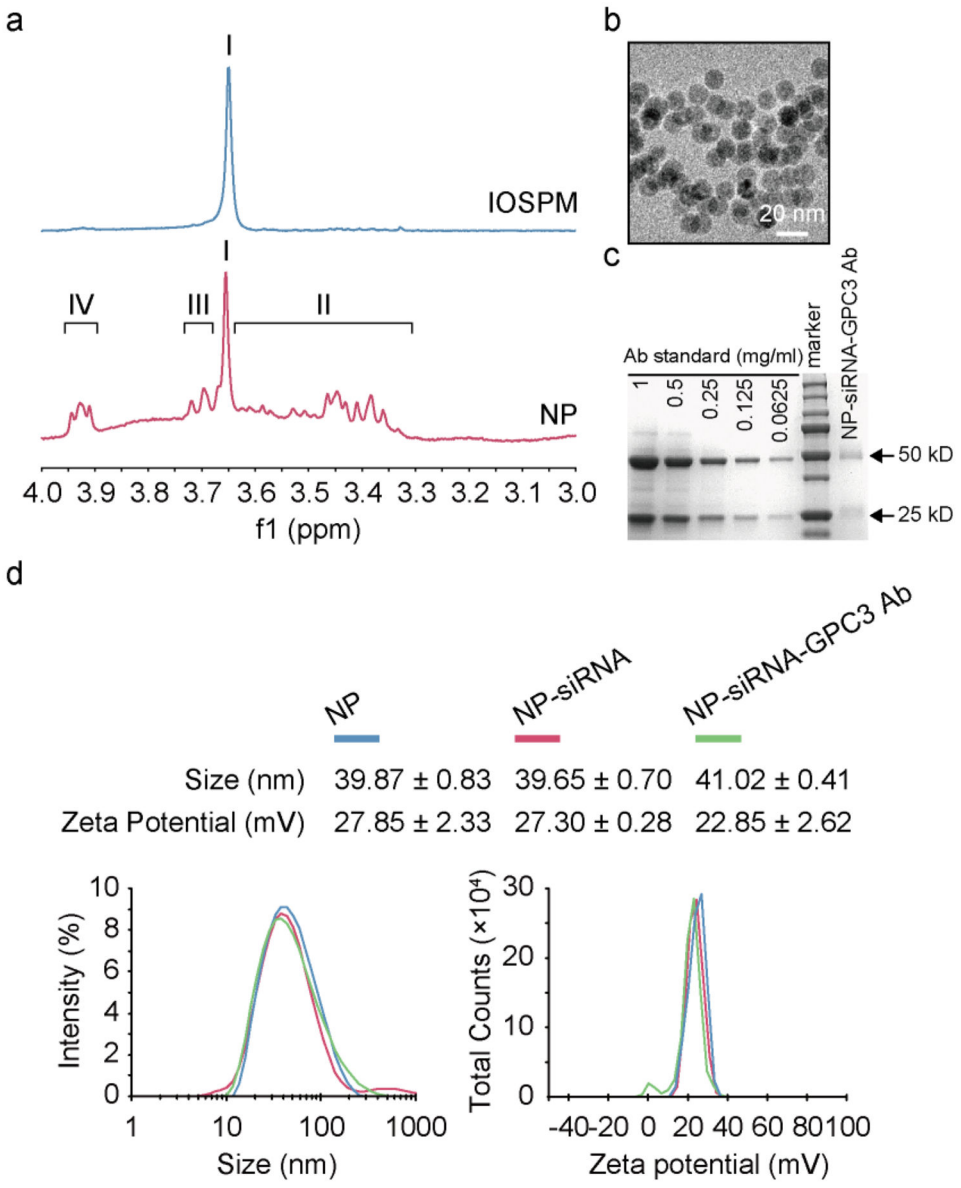

Figure 2.

Characterization of NP-siRNA-GPC3 Ab. (a) 1H-NMR analysis of IOSPM and NP. The characteristic peak of the ethylene group of PEG (peak I) on IOSPM, the ethylenimine group of PEI (peak II), and 6 peaks of aldohexoses (peak III and IV) on chitosan were indicated on spectrum of NP. (b) TEM images of NP-siRNA-GPC3 Ab; scale bar = 20 nm. (c) SDS-PAGE image showing the presence of Ab on NP-siRNA-GPC3 Ab with free Ab used as the standard. (d) Hydrodynamic size and zeta-potential of NP, NP-siRNA, and NP-siRNA-GPC3 Ab at pH 7.4 as determined by DLS.

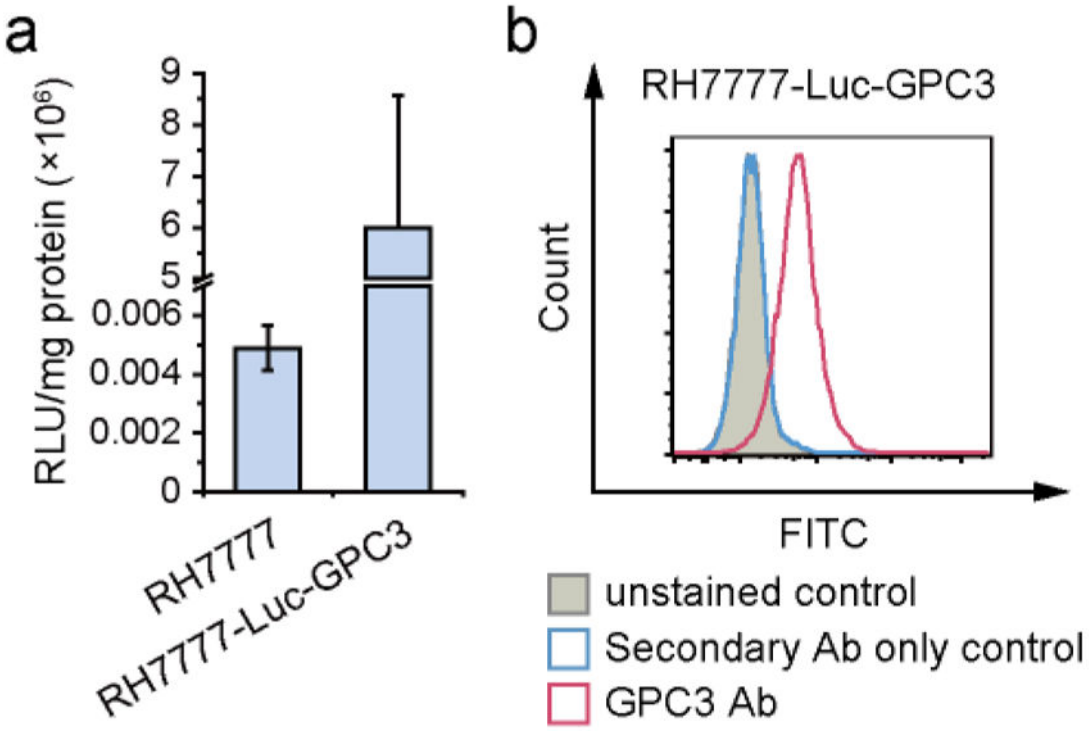

Figure 3.

Characterization of RH7777-Luc-GPC3 cells. (a) Evaluation of Luc activity of RH7777-Luc-GPC3 cells using *in vitro* Luc assay, where native RH7777 cells served as negative control. (b) Flow cytometry analysis of GPC3 expression in RH7777-Luc-GPC3 cells. Filled peak represents unstained control. Histograms for secondary Ab control are also shown.

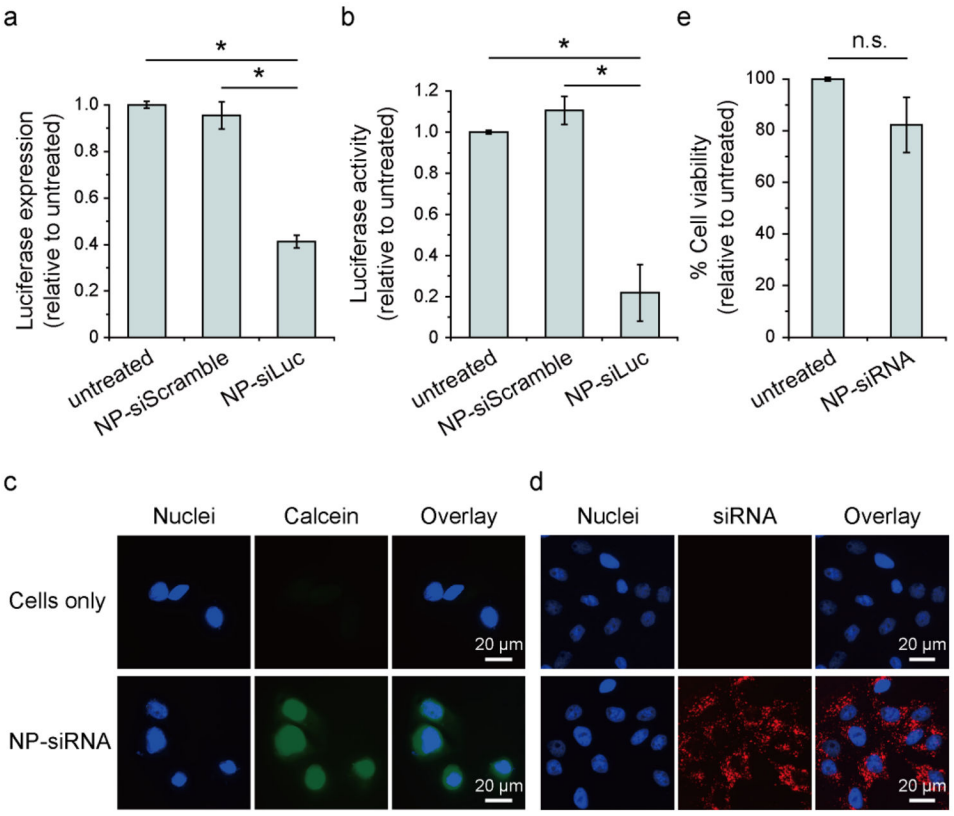

Figure 4.

Effective suppression of Luc in RH7777-Luc-GPC3 cells by NP-siLuc transfection *in vitro*. (a) Knockdown of Luc mRNA in RH7777-Luc-GPC3 cells quantified by qRT-PCR. (b) Suppression of Luc protein in RH7777 cells as a result of NP-siLuc treatment. (c) Fluorescence images of RH7777-Luc-GPC3 cells treated with calcein (top row) and cells treated with NP-siRNA-GPC3 Ab and calcein mixture (bottom row). (d) Fluorescence images of RH7777-Luc-GPC3 cells transfected with fluorophore-labeled NP-siRNA. (e) RH7777-Luc-GPC3 cell viability after NP-siLuc treatment; * indicates statistical significance ($P < 0.05$) and n.s. indicates no statistical significance as determined by Student's *t*-test.

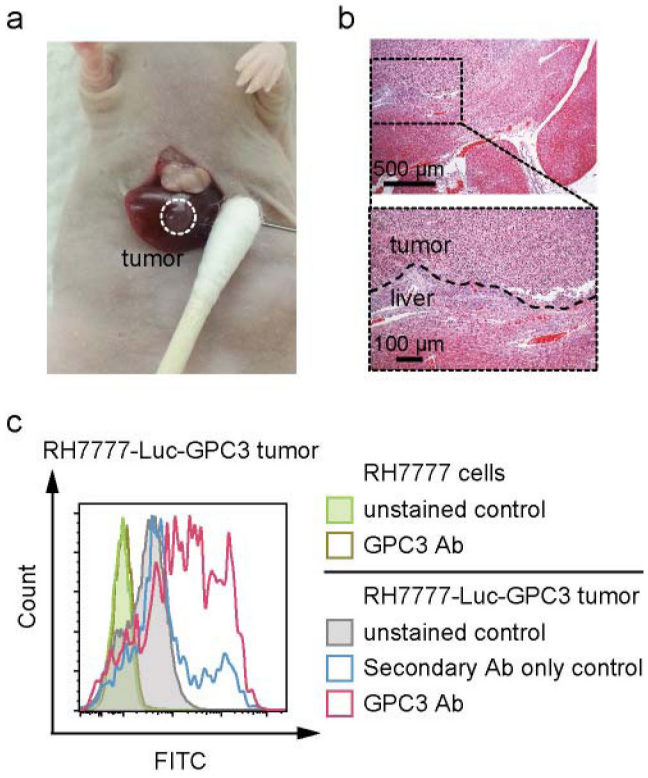

Figure 5.

Characterization of orthotopic RH7777-Luc-GPC3 xenografts. (a) Photograph of RH7777 tumor implantation. The xenograft is recognized as a solitary nodule protruding from the liver surface. (b) Histological characteristics of the RH7777 tumor sections evaluated by H&E staining. (c) Representative flow cytometry analysis of GPC3 antigen displayed on the cell surface. Filled peaks represent unstained controls of RH7777 cells and RH7777-Luc-GPC3 tumor. Histograms for secondary Ab control are also shown.

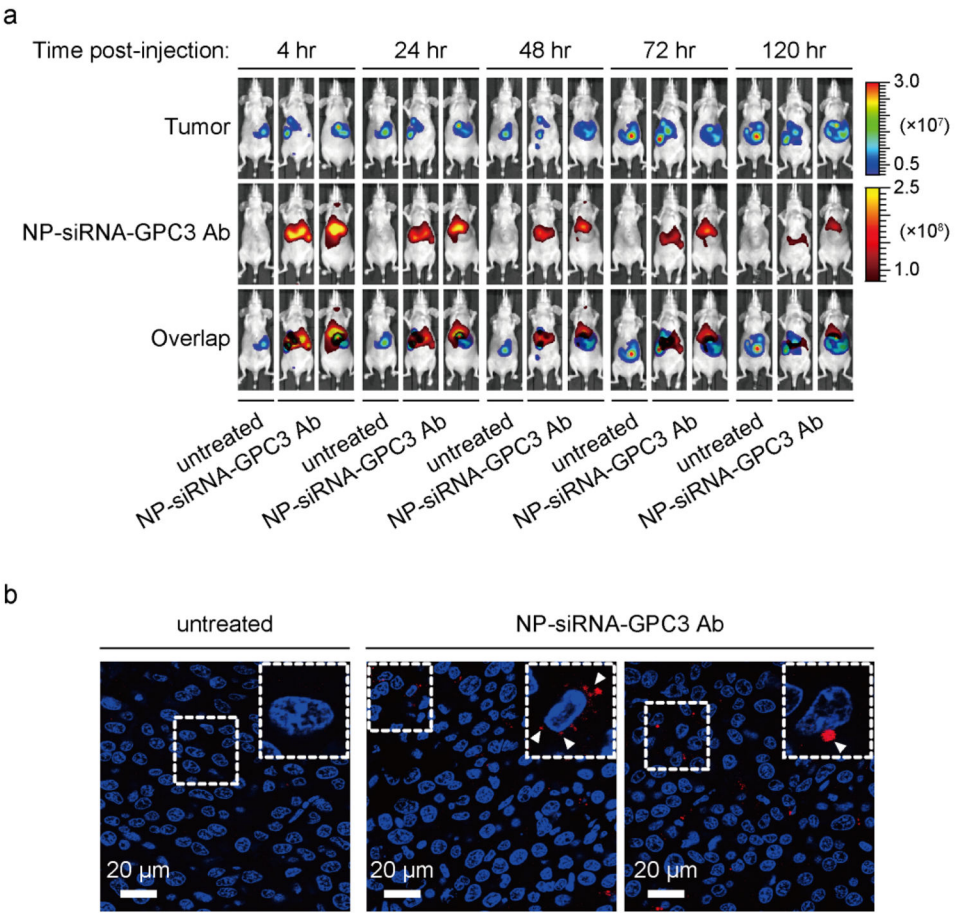

Figure 6.

Evaluation of tumor uptake of NP-siRNA-GPC3 Ab *in vivo*. (a) Xenogen IVIS images showing co-localization of RH7777-Luc-GPC3 tumor and Dy677-labeled siRNA loaded NP at different time points post-injection from one untreated and two treated mice. (b) Confocal fluorescence microscopy images showing accumulation of NP-siRNA-GPC3 Ab in tumor sections at 120 hr after injection from the same animals presented in panel (a).

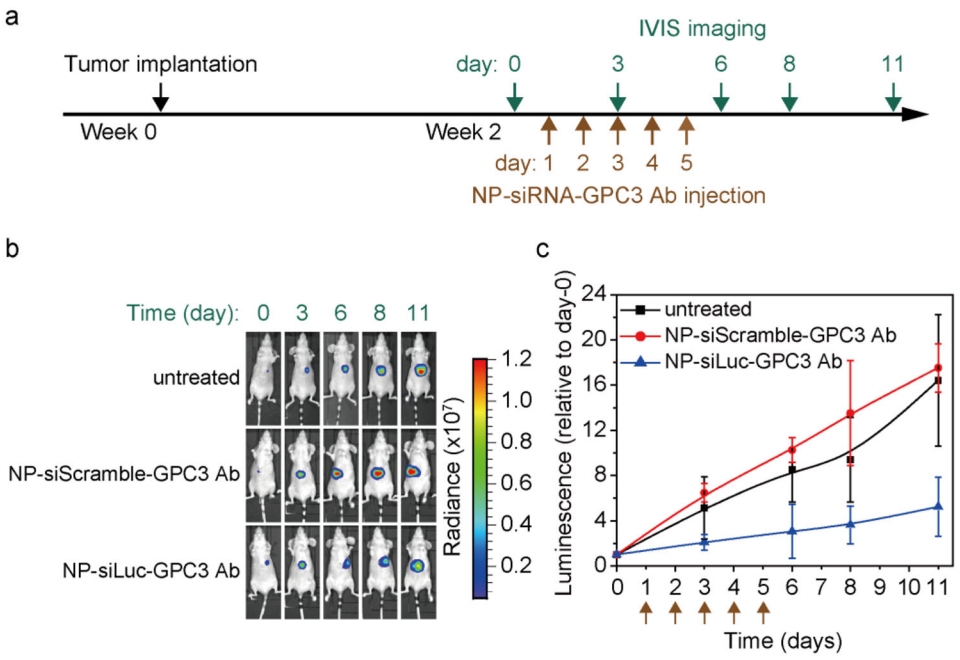

Figure 7.

In vivo delivery of NP-siLuc-GPC3 Ab knocks down luminescence of RH7777-Luc-GPC3 tumors. (a) Scheme of tumor implantation and treatment. Two weeks after orthotopic injection with RH7777-Luc-GPC3 cells, xenograft-bearing mice received five daily intravenous injections of NP-siLuc-GPC3 Ab. IVIS imaging was initiated one day prior to the first NP-siLuc-GPC3 Ab injection. (b) Representative live IVIS images of mice bearing RH7777-Luc-GPC3 tumors with administration of NP-siLuc-GPC3 Ab. Untreated mice and mice treated with scramble siRNA served as the controls. (c) Quantitative luminescence of mice from untreated and treated groups (n = 4). Luminescence was normalized to day 0 and line graph was indicated as presented as mean ± SD. Arrows indicate NP-siRNA-GPC3 Ab injection.